ENVIRONMENTAL RESEARCH
LETTERS

PURPOSE-LED PUBLISHING™ Part of the ENVIRONMENTAL RESEARCH SERIES

LETTER • OPEN ACCESS

Brucite-inspired ocean alkalinity enhancement alters the biogeochemistry and composition of a phytoplankton community: a Santa Barbara channel case report

To cite this article: Zoë S Welch *et al* 2025 *Environ. Res. Lett.* **20** 114087

ENVIRONMENTAL RESEARCH
LETTERS

OPEN ACCESS

RECEIVED
30 November 2024

REVISED
18 October 2025

ACCEPTED FOR PUBLICATION
24 October 2025

PUBLISHED
11 November 2025

LETTER

Brucite-inspired ocean alkalinity enhancement alters the biogeochemistry and composition of a phytoplankton community: a Santa Barbara channel case report

Zoë S Welch[1,2,*], Sylvia M Kim[1,2], Michael Liu[1], An Bui[1,3], Jesse Grigolite[3], Janice L Jones[2] and M Débora Iglesias-Rodríguez[1,2]

[1] Department of Ecology, Evolution, and Marine Biology, University of California Santa Barbara, Santa Barbara, CA 93106, United States of America
[2] Marine Science Institute, University of California Santa Barbara, Santa Barbara, CA 93106, United States of America
[3] Department of Environmental Studies, University of California Santa Barbara, Santa Barbara, CA 93106, United States of America
[*] Author to whom any correspondence should be addressed.

E-mail: zoe.welch@lifesci.ucsb.edu

Keywords: marine carbon dioxide removal (mCDR), ocean alkalinity enhancement (OAE), phytoplankton, climate change, marine calcification, silicification, marine biogeochemistry

Supplementary material for this article is available online

Abstract

The dramatic impacts of global climate change have driven marine carbon dioxide removal innovation, including ocean alkalinity enhancement (OAE), in an attempt to keep global warming under 2 °C. We conducted a laboratory experiment to assess the impacts of brucite inspired alkalinity addition (BIAA) as an OAE approach on the carbonate chemistry, biogeochemistry, and composition of the natural Santa Barbara Channel phytoplankton community sourced from a spring upwelling event. The BIAA treatment used $MgCl_2$ * $6H_2O$ and NaOH to yield a total alkalinity (TA) concentration of ∼3000 μmol kg^{-1}, in contrast with the untreated seawater controls (TA = ∼ 2300 μmol kg^{-1}). Our results suggest that BIAA altered the phytoplankton community composition, including reduced contribution of diatoms and enhanced numbers of Prymnesiophyceae (coccolithophores and *Phaeocystis* sp.). These results are in agreement with observations that biogenic silica content was lower under BIAA treatment. While the concentration of particulate inorganic carbon was consistently higher compared to controls, these differences were not statistically significant. Results revealed no differences between control and BIAA treatment in particulate organic carbon and particulate organic nitrogen (PON) concentrations. The proxy for cellular photosynthetic health F_v/F_m revealed that cells were photosynthetically healthy for both control and BIAA treatments, but values were lower in the BIAA treatment at the beginning of the exponential phase. While statistical power limitations of laboratory results might restrict applicability to other systems, our overall results suggest that BIAA has a differential impact on phytoplankton functional groups and their biogeochemical performance.

1. Introduction

Accelerated increases in atmospheric carbon dioxide concentrations [1] brought about by anthropogenic activities [2–4] have led to global climate disturbance and ocean acidification [5, 6]. Ocean alkalinity enhancement (OAE) is a marine carbon dioxide removal (mCDR) approach that relies on the addition of alkalinity to seawater in order to promote atmospheric CO_2 drawdown and potentially temporarily combat local ocean acidification [7].

Our understanding of the effects of OAE on marine microbes remains however in its infancy. From laboratory experiments using different OAE approaches, we know that OAE can variably alter cellular photosynthetic efficiency [8–10]. In contrast,

other functions like silicic acid drawdown and biogenic silica (BSi) 'build-up' have been shown to decline under added $NaHCO_3$ and NaOH mesocosm conditions [11], with reduction in silicic acid drawdown also being observed in monospecific *Chaetoceros* sp. cultures with Na_2CO_3 and $CaCl_2H_4O_2$ addition [8]. Further, applying OAE has been shown to increase the biological variability within a system, as evidenced by differences in phytoplankton community gene expression [10], composition [9, 10] and perturbation of the temporal trends of key biogeochemical parameters like particulate organic carbon (POC):PON [11].

One of the candidate materials identified for OAE is brucite, a mineral form of $Mg(OH)_2$, which can be sourced as a byproduct of industrial processes as well as mined from widely distributed terrestrial sites around the globe [12–14]. Theoretically, every mol of brucite dissolved can remove 2 moles of CO_2 from the atmosphere equation (1), increasing alkalinity by 2 mole equivalents [15],

$$Mg(OH)_2 + 2CO_2 \Leftrightarrow Mg^{2+} + 2HCO_3{}^{-}. \quad (1)$$

The efficiency of brucite CO_2 removal is critically dependent on temperature, salinity [16], gas exchange, and surface residence time [17].

The biological impacts of OAE using Mg-based alkali remain an open question. Experimental data are very limited, with only a study by Delacroix *et al* examining the impacts of solid-phase $Ca(OH)_2$, NaOH, or $Mg(OH)_2$ on a natural microalgal assemblage from a Norwegian fjord as well as cultures of *Tetraselmis suecica* (green microalga) and *Skeletonema costatum* (diatom) [18]. The authors found $Mg(OH)_2$ to have low toxicity compared to $Ca(OH)_2$ and NaOH, as assessed via measurements of growth inhibition and survival percentage [18]. Biogeochemical modeling work by Fakhraee *et al* concluded that metal oxide-based materials such as MgO and $Mg(OH)_2$ may have significant mCDR potential, though altered marine particle cycling associated with the biological carbon pump may occur [7].

In this study, we examined the effects of OAE via brucite inspired alkalinity addition (BIAA) on the seawater carbonate chemistry and phytoplankton community biogeochemistry, physiology, and composition during a spring upwelling event in the Santa Barbara channel (SBC). Specifically, our aim was to describe changes through time in the abiotic and biotic components of the system due to alkalinity addition (though see Dickson *et al* [19] for analysis of the relationship between alkalinity and dissolved inorganic compounds). The SBC is a highly productive system within the California Current Large Marine Ecosystem, undergoing seasonal upwelling [20, 21] and historically experiencing high variability in multiple abiotic parameters (e.g. dissolved oxygen [22, 23], nutrients [23, 24], temperature [25–27], and pH [23, 25, 28]). Additionally, recent work has demonstrated that abrupt changes to carbonate chemistry are realistic under different OAE addition scenarios [8, 17]. Thus, it is crucial to undertake experimentation that provides insight into alkalinity addition effects at the site of deployment, incorporating naturally variable conditions into experimental design. Results from this laboratory experiment contribute to understanding chemical and biological responses in a high CO_2 coastal environment that may be subject to 'hot spot' alkalinity-addition conditions [29, 30]. Though limited statistical power is inherent to data generated in lab studies, our results contribute important perspective to the rapidly-evolving field of OAE research and implementation.

2. Methods

2.1. Experimental setup

Seawater was collected on 10 May 2023 from the SBC (34.3 °N, 119.8 °W) and filtered twice through a 200 μm Nylon mesh to exclude large zooplankton. Following Gately *et al* [8], we added nutrients to achieve final concentrations of 100 μm nitrate, 6.24 μm phosphate, 70 μm silicate, and vitamins and minerals in f/2 concentrations (Guillard and Ryther ; Langer *et al*) in the treatments to ensure nutrient-repletion [31, 32]. For the abiotic treatments, seawater was further filtered through a 0.2 μm polyethersulfone filter. Experimental treatments were conducted in 1 l volumes using 2 l polycarbonate vessels, and all cultures were aerated by bubbling with air containing a CO_2 partial pressure of 420 μatm (Airgas).

The BIAA treatment mimicked the dissolution of brucite ($Mg(OH)_2$) in seawater to achieve a total alkalinity (TA) concentration in seawater of ~3000 μmol kg^{-1} [8, 29, 33] using 0.1 M $MgCl_2$ * $6H_2O$ and 0.1 M NaOH. Because of the extremely slow and incomplete dissolution of $Mg(OH)_2$, we did not use this mineral form. We refer to the alkalinity-added treatments as **BIAA-A** and **BIAA-B**, while those without addition are **Control-A** and **Control-B** ('A' and 'B' designating abiotic and biotic, respectively).

All treatments were kept at 12–15 °C under a light irradiance of ~170 μmol photons m^{-2} s^{-1} with a light/dark (16 h/8 h) cycle using cool white fluorescent lighting. Sampling was conducted in triplicate using sacrificial replication [33] during the same time window on every third day of the experiment (days 0, 3, 6, 9, and 12).

2.2. Chemical analyses

2.2.1. Carbonate chemistry

We sampled seawater in accordance with established carbonate chemistry best practices [34], and measured pH [35],TA, salinity, dissolved phosphate

and silicate, and temperature in order to calculate the remaining carbonate chemistry parameters using CO2Sys (v2.1) [36] applying the total pH scale and equilibrium constants from Mehrbach *et al* refit by Dickson and Millero [37, 38]. Samples were kept in 250 ml airtight borosilicate bottles containing 100 μl of supersaturated $HgCl_2$ solution to prevent biological activity from altering the carbonate chemistry of the sample.

2.2.2. Particulate matter

POC and particulate organic nitrogen (PON) were sampled by collecting 200 ml samples followed by filtration and storage until analysis [8] at UC Santa Barbara's Marine Science Institute (MSI) Analytical Lab. We used inductively coupled plasma optical emission spectroscopy (ICP-OES) to analyze the calcium (Ca) associated with the natural phytoplankton assemblage, representative of particulate inorganic carbon (PIC). Briefly, we filtered 150 or 200 ml of cultures through a 0.2 μm polycarbonate Isopore™ filter. For ICP-OES analysis of particulate matter, we then transferred each filter to a separate 50 ml Falcon tube which was stored at −20 °C until processing. We processed the samples by adding 50 ml of 0.1 M nitric acid, and the acidified filters were gently shaken overnight at 15 °C. The solution was subsequently filtered through a 0.45 μm Whatman polyethersulfone filter (Puradisc) into new 50 ml centrifuge tubes. Samples were analyzed at UC Riverside's Environmental Sciences Research Lab (ESRL) using a PerkinElmer Optima 7300DV instrument.

2.2.3. Elemental chemistry

We collected triplicate samples to analyze dissolved Ca, magnesium (Mg), and sodium (Na) in seawater via ICP-OES. Samples were stored at 4 °C until processing at UC Riverside's ESRL. Correction for potential seawater contamination (residual Ca) on our filters for PIC analysis was conducted by analyzing dissolved Na concentrations [39].

2.2.4. Dissolved inorganic nutrients

We collected triplicate samples for dissolved inorganic nutrient (silicate, phosphate, and nitrite + nitrate) analysis via flow injection analysis (FIA). Samples were sourced from the same filtrate pool used to source the ICP-OES dissolved fraction samples. FIA samples were stored at −20 °C until processing using a Lachat QuikChem 8000 Series 2 FIA instrument (Zellweger Analytics) at UC Santa Barbara's MSI Analytical Lab.

2.2.5. BSi

We obtained triplicate 100 ml samples for BSi by gentle filtration through 0.4 μm polycarbonate Isopore™ filters. Filters were then transferred to 15 ml centrifuge tubes (Olympus Plastics) and stored at −20 °C until processing via NaOH digestion and subsequent colorimetric spectrophotometry (ThermoFisher Genessys 30 VIS) analysis [40–42].

2.2.6. Scanning electron microscopy with energy dispersive x-ray spectroscopy (SEM-EDX)

We collected samples for SEM-EDX from abiotic treatments on days 6 and 12 to assess potential formation of precipitates and their composition. Samples were filtered gently through 0.4 μm polycarbonate Isopore™ filters which were then dried and stored at room temperature until processing at the SEM laboratory of the Santa Barbara Museum of Natural History using a Zeiss EVO 10 LS with Zeiss EDS detector and paired Smart EDX software.

2.3. Biological analyses

2.3.1. Photosynthetic properties

We utilized an Aquapen-C AP 110-C fluorometer to measure photosynthetic parameters including variable (F_v) and maximum (F_m) fluorescence to determine F_v/F_m, an indicator of quantum efficiency of photosystem II, which is a proxy for cellular photosynthetic health. We also measured FixArea, which is a proxy indicator for chlorophyll *a* content. All measurements on the samples were conducted under OJIP settings [43–47] following 20 min of dark adaptation.

2.3.2. Phytoplankton community composition and growth

We collected triplicate 45 ml samples for microscopic taxonomic identification and enumeration of phytoplankton cells. Cells were fixed in 3.9% formalin and samples were stored at 4 °C until processing. An Olympus BX53 light microscope was used for cell identification and counting to calculate phytoplankton cell densities. The phytoplankton community reached exponential growth by day 3 and this phase continued to day 9 (figures 2 and 4).

2.4. Data analysis

Statistical analysis and figure generation were performed in R (version 4.3.2; 2023–10-31) using RStudio Build 494 (2023.09.1).

To determine the effects of treatment (Control-A, Control-B, BIAA-A, BIAA-B) within a given sampling day on carbonate chemistry parameters TA, pH, TCO_2, $[CO_2]$, HCO_3^-, and CO_3^{2-}, we used Kruskal–Wallis tests ($n\alpha$ 3 per treatment-day). If we detected significant differences from the initial Kruskal–Wallis tests (α 0.05 for all statistical tests), we conducted post-hoc Conover-Iman tests for pairwise comparisons. We determined the magnitude of effects using Cliff's δ following Meissel and Yao [48].

To determine differences in biogeochemistry and physiology between biotic treatments (Control-B and BIAA-B) across time on the biogeochemical and physiological parameters BSi, POC, PIC, PON,

F_v/F_m, and FixArea, we used aligned rank transform (ART) ANOVA tests [49, 50] to examine the interactive effects of biotic treatment and sampling day ($n = 3$ per treatment-day). If we detected significant differences amongst biotic treatments and day, we conducted post-hoc Tukey Honestly Significant Difference tests to determine significantly different pairwise comparisons. We determined the magnitude of differences across biotic treatments and sampling day using partial η^2 following Cohen [51].

To describe differences between group (i.e. dinoflagellate, diatom, coccolithophore, and *Phaeocystis* spp.) abundance between biotic treatments (Control-B and BIAA-B), we calculated mean and standard error of counts from light microscopy for each individual group within each treatment for each sampling day. To describe total differences across biotic treatments, we calculated mean and standard error of counts across biotic treatments for the total phytoplankton community for each sampling day. To compare the proportional contribution of each group to the total phytoplankton community, we calculated the proportion of group counts for each treatment for each day.

3. Results

3.1. Seawater carbonate chemistry

BIAA presence yielded significant TA differences between the controls and BIAA treatments (figure 1(a)), with BIAA treatments consistently having higher TA than control treatments. Unlike TA, seawater pH was highly variable through time across all treatments. In the BIAA treatments, pH decreased from day 0 to day 3 while by day 6, the abiotic and biotic treatments diverged, with seawater pH in BIAA-A continuing to decrease while steadily increasing in BIAA-B until the end of the experiment (figure 1(b)). In non-BIAA-treated controls, seawater pH in Control-B greatly increased, significantly diverging from Control-A by day 3 ($H = 9.67$, $p = 0.02$, $\delta = -1$, t = 0.02) and continued to linearly increase throughout the duration of the experiment. Notably, seawater pH began to converge in both Control and BIAA biotic treatments by day 12; abiotic treatments demonstrated similar convergence.

The TCO_2 concentration for BIAA-A and BIAA-B increased until day 3. By day 6, TCO_2 continued to increase in BIAA-A while it decreased comparatively until day 9 in BIAA-B. TCO_2 differences between BIAA-A and BIAA-B on day 6 were significant ($H = 10.39$, $p = 0.02$, $\delta = -1$, $t = 0.01$), and remained so until the end of the experiment. By day 6 onwards, TCO_2 concentrations were significantly lower in the biotic treatments (Control-B or BIAA-B) compared to their abiotic counterparts (figure 1(c)). CO_2 and HCO_3^- in the abiotic treatments increased through time. In the BIAA-A treatment, after an initial ∼sixfold drop in CO_2 compared to controls, CO_2 increased steadily to levels comparable to those of controls at time 0 (∼12 μmol kg^{-1}). In Control-A, CO_2 levels increased steadily from time 0 to reach values of ∼15 μmol kg^{-1} (figure 1(d)). HCO_3^- in BIAA-A experienced an initial 23% decrease compared to controls, and then increased (+64%) over the duration of the experiment, with HCO_3^- concentrations in BIAA-A surpassing those of Control-A by day 9 (figure 1(e)). HCO_3^- and CO_2 declined steadily in Control-B through time, whereas there was a moderate decrease of 7% and 20%, respectively in BIAA-B (figures 1(d) and (e)). Conversely to HCO_3^- and CO_2, CO_3^{2-} in BIAA-A declined by 59% by the end of the experiment. In Control-A, CO_3^{2-} declined by approximately 17% by the end of the experiment. CO_3^{2-} in BIAA-B experienced an initial decrease of 17% from day 0 to day 3, in contrast with a 20% increase in Control-B over the same time frame. After day 3, the concentration of CO_3^{2-} in both BIAA-B and Control-B increased by 31% and 93%, respectively.

3.2. Biogeochemical and physiological impacts

BSi, POC, PIC and particulate organic nitrogen (PON) increased over the course of the experiment in both Control-B and BIAA-B (figures 2(a)–(d)). BSi levels were lower in BIAA-B relative to Control-B, with this corresponding to a large and statistically significant treatment effect (Pr(>F) and $p = 0.015$; $\eta^2 = 0.26$). PIC values were slightly higher in BIAA-B compared to Control-B throughout the course of the experiment, but differences did not correspond to a statistically significant treatment effect (Pr(>F) and $p = 0.187$; $\eta^2 = 0.09$). By the end of the experiment, POC, PIC and PON in BIAA-B and PIC and PON in Control-B seemed to have entered a plateau, suggesting that the protist community had entered the stationary phase of growth. The maximum potential quantum efficiency of Photosystem II, F_v/F_m (figure 2(e)) peaked during exponential phase at values of around 0.65 indicative of nutrient-replete, healthy cells [52] in both BIAA-B and Control-B though there was an observed lag in F_v/F_m values in BIAA-B compared to Control-B during the day 3 transitory timepoint. On day 3, lower values in BIAA-B compared to Control-B were observed in five of the six biogeochemical and physiological parameters measured: BSi (43%), POC (51%), PON (52%), F_v/F_m (10%), and FixArea (74%). Average F_v/F_m values were 10% lower on days 3 and 9 in the BIAA treatment compared to the control, with BIAA presence causing small and significant alteration to F_v/F_m over the course of the experiment (Pr(>F) and $p = 0.034$; $\eta^2 = 0.21$). With the advent of stationary phase, a drop of 20%–22% in the average value of F_v/F_m was observed in both BIAA-B and Control-B, and drops of ∼60% (BIAA-B) and ∼36% (Control-B) were seen in FixArea, a proxy indicator of chlorophyll a content (figures 2(e) and (f)).

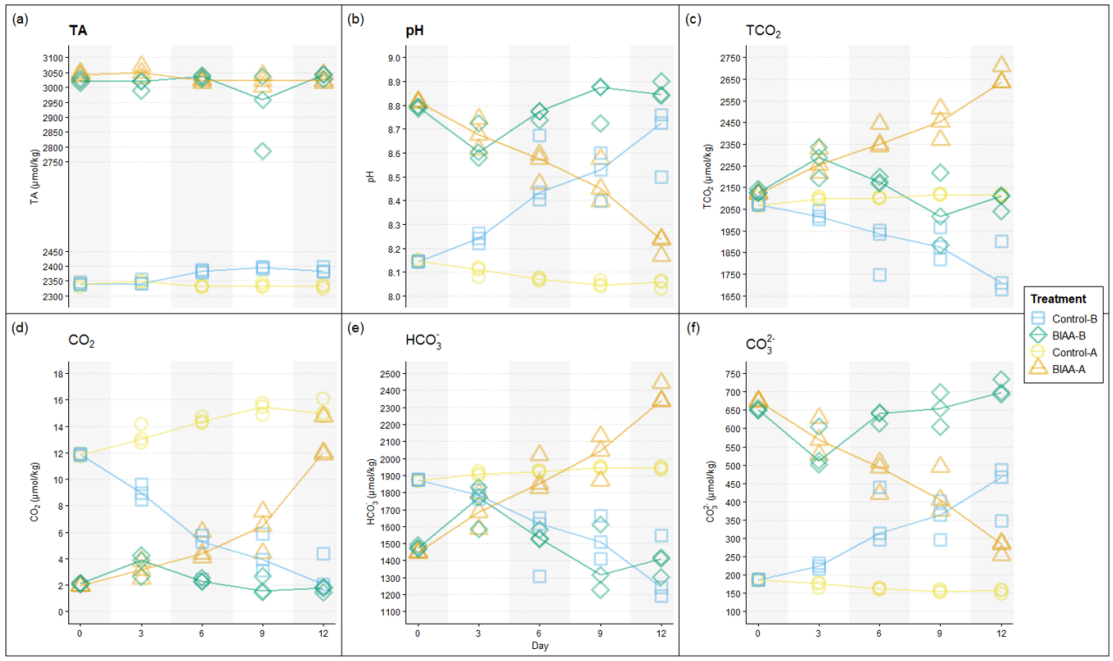

Figure 1. Carbonate chemistry parameters: (a) TA, (b) pH, (c) TCO_2, (d) $[CO_2]$, (e) HCO_3^-, and (f) CO_3^{2-} over time across all 4 treatments (Control-A: yellow circles, Control-B: blue squares, BIAA-A: orange triangles, BIAA-B: green diamonds). Open symbols indicate replicates ($n = 3$ per treatment-day).

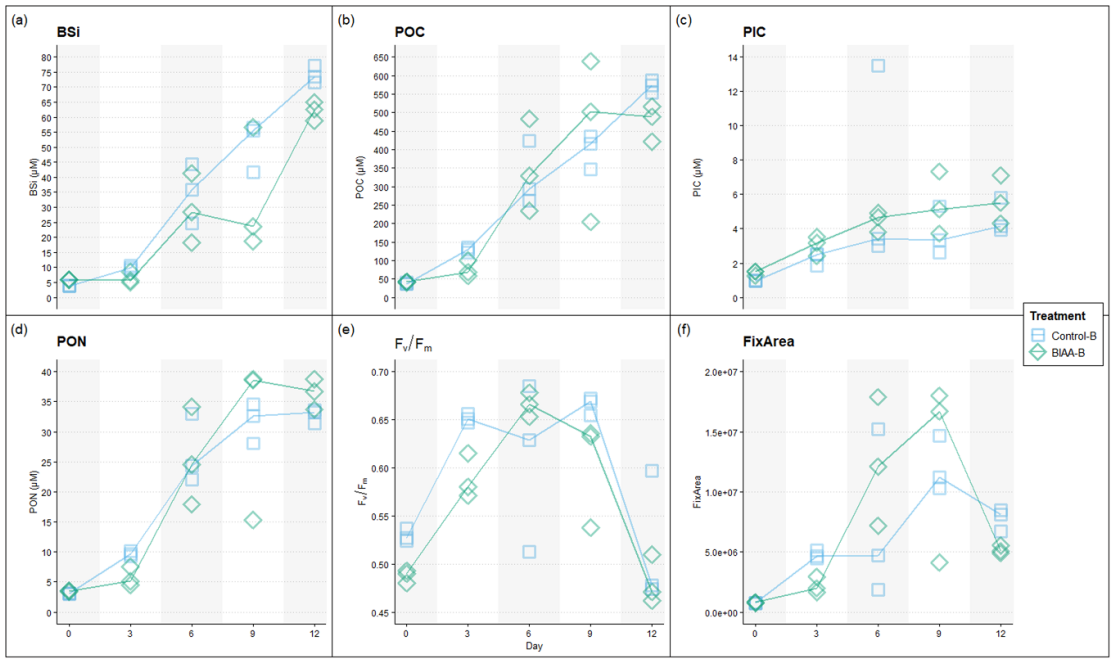

Figure 2. Biogeochemical and physiological parameters (a) BSi, (b) POC, (c) PIC, (d) PON, (e) F_v/F_m, (f) FixArea over time in Control-B (blue squares) and BIAA-B (green diamonds). Open symbols indicate replicates (n = 3 per treatment-day).

The PIC:POC ratio (figure S1(b)), which can be used as a proxy to determine whether the protist community acts as a source (>1) or sink (<1) of CO_2 to the environment, did not vary appreciably between Control-B and BIAA-B over the duration of the experiment, with all values remaining <1. Overall, broad patterns for biogeochemical ratios (BSi:POC, PIC:POC, POC:PON) appear to be conserved between Control-B and BIAA-B, with temporal variability in POC:PON ratios observed between the treatments during the stationary phase.

3.3. Dissolved inorganic nutrients

We observed silicate, phosphate, and nitrite + nitrate drawdown in both biotic treatments although the patterns and extent of drawdown differed slightly

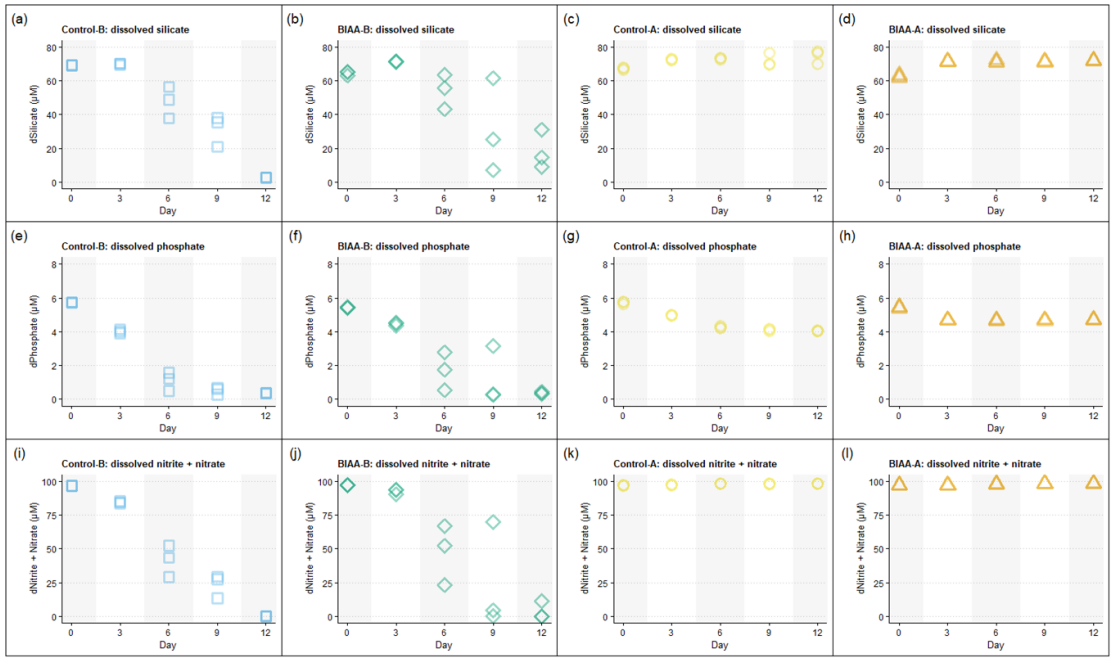

Figure 3. Dissolved inorganic nutrients (silicate, phosphate, and nitrite + nitrate) in seawater over time across all 4 treatment levels (Control-A: yellow circles, Control-B: blue squares, BIAA-A: orange triangles, BIAA-B: green diamonds). Open symbols indicate replicate measurements (n = 3 per treatment-day) from flow injection analysis.

between controls and BIAA treatments. During the exponential phase (days 3–9), there was a greater removal of nitrite + nitrate and silicate in BIAA-B compared to Control-B, but a greater removal of phosphate in Control-B than in BIAA-B. In Control-B, nitrite + nitrate and silicate were fully depleted by day 12, and phosphate was depleted by day 9. In BIAA-B, nitrite + nitrate and phosphate were depleted in a majority of replicates by day 9, while silicate did not appear to be fully depleted. Comparison of silicate trends between Control-B and BIAA-B (figures 3(a) and (b)) show linear silicate drawdown in Control-B with relatively low variability across replicates, while in BIAA-B silicate removal appeared to be non-linear and showed a higher degree of variability across replicates. We observed comparable (<5% difference) values for nitrite + nitrate and phosphate in Control-B and BIAA-B while a greater drawdown in silicate (96.17%) was observed in Control-B compared to BIAA-B (71.86%).

In the abiotic treatments, we only observed a slight decrease in phosphate concentration over time. The dissolved phosphate trendlines in both Control-A and BIAA-A had comparable slopes over the experiment's duration, and similar final phosphate concentrations on day 12 (figures 3(g)–(h)) coincident with decreasing pH over time for both Control-A and BIAA-A (figure 1(b)). Further, the comparable slopes and final phosphate concentrations in Control-A and BIAA-A (figures 3(g)–(h)), despite the difference in pH reduction from day 0 to day 12 seen in Control-A (pH 7.99–7.91) and BIAA-A (pH 8.65–8.07), may be explained by the ability of Mg presence to significantly inhibit the growth of precipitates composed of phosphate and Ca [53–55].

3.4. Phytoplankton community structure

Although no apparent changes in productivity were observed (figure 2(b) and (f)), our results revealed differences in the phytoplankton community composition in the BIAA treatment compared to the control; notably, the relative abundance of phytoplankton functional group representatives including diatoms (Bacillariophyceae), dinoflagellates (Dinoflagellata *incertae sedis*), and coccolithophores and *Phaeocystis* spp. (Prymnesiophyceae).

The phytoplankton community abundance differed between BIAA-B and Control-B throughout the experiment, with lower overall average cell counts in BIAA-B compared to Control-B (figure 4(b)). Phytoplankton community cell abundance was ∼90% lower in BIAA-B compared to Control-B at the start of exponential phase (day 3), and while this difference became smaller throughout the remainder of exponential phase, community abundance remained ∼7% lower in BIAA-B compared to Control-B on both day 6 and 9 (figure 4(b)).

In the BIAA treatment, we observed notable differences in the phytoplankton community structure compared to the control (figure 4). The community was dominated by diatoms but the BIAA treatment resulted in a reduced contribution of diatoms to the phytoplankton community compared to Control-B. Conversely, the relative abundance of

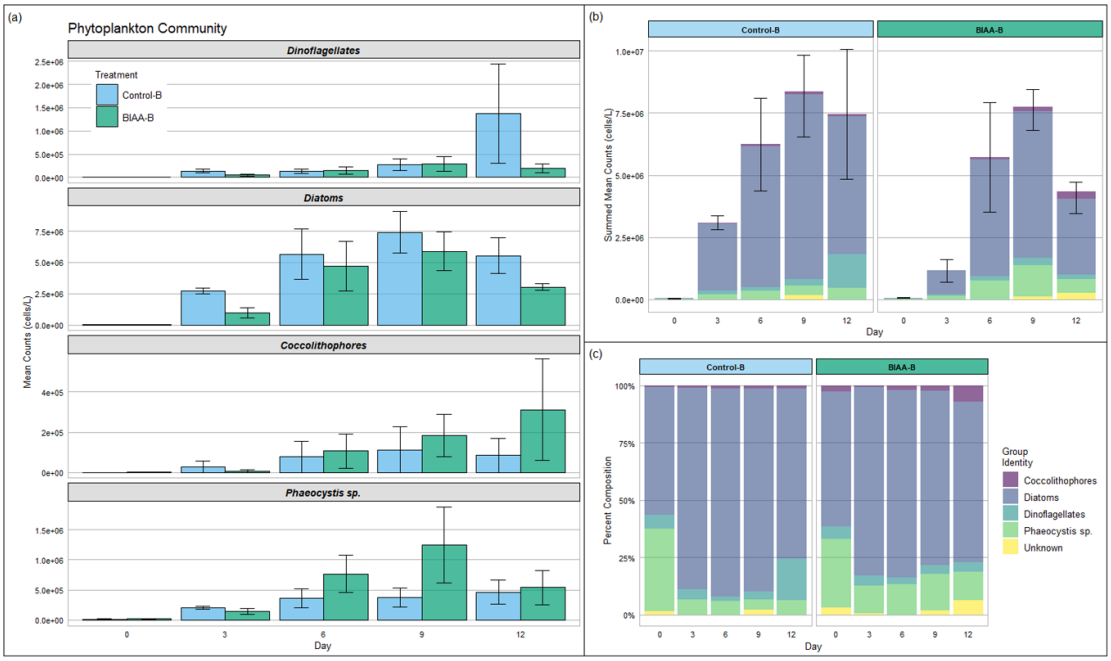

Figure 4. Phytoplankton relative community abundance and composition assessed via light microscopy. All mean counts for a given treatment-day were calculated by binning results from triplicate samples. (a) Dinoflagellates, diatoms, coccolithophores, and Phaeocystis spp. mean counts differ over time. Control-B: blue; BIAA-B: green. (b) Relative composition and abundance of the phytoplankton community differ over time within Control-B versus BIAA-B. For (a), black bars represent standard error of the group cell counts for a given day, and for (b) black bars represent standard error of the whole community cell counts for a given day. (c) Percent composition of the Control-B versus BIAA-B phytoplankton community differ over time. For both (b) and (c), community member identification was binned as coccolithophores (purple), diatoms (periwinkle), dinoflagellates (aqua), Phaeocystis spp.(green), and unknown (yellow).

Prymnesiophyceae (coccolithophores and *Phaeocystis* spp.) appeared to be higher in BIAA-B compared to Control-B throughout the course of the experiment. The response of dinoflagellates was less clear as no distinct relative abundance trend was observed throughout the experiment, and the difference between Control-B and BIAA-B on day 12 could not be parsed from potential confounding nutrient limitation effects (figures 3(a), (b), (e), (f), (i) and (j)) [33, 56].

4. Discussion

4.1. Changes in carbonate chemistry

Our POC and F_v/F_m results indicate a healthy, active protist community consistent with the drawdown of CO_2 and HCO_3^- in biotic treatments. Biological activity exerted a strong influence on pH, with a distinct increasing pattern driven by photosynthetic CO_2 fixation during the exponential phase of growth, in contrast with abiotic treatments, which follow general trends of pH decrease (−0.1 units for Control-A and −0.59 units for BIAA-A) (figures 1 and 2). In biotic treatments, pH and CO_3^{2-} increased over time, in contrast with the decline observed in abiotic treatments. The opposite trend—decreases in biotic treatments and increases in abiotic treatments—were observed for TCO_2, CO_2, and HCO_3^- (figure 1). Moreover, from day 3, during the exponential phase of growth, photosynthesis exerts a strong influence on carbonate chemistry. Interestingly, while TCO_2 removal trends were comparable between BIAA-B and Control-B during exponential phase, TCO_2 concentrations were similar at the start and end of the experiment for BIAA-B whereas TCO_2 concentrations decreased by ∼15% over the course of the experiment for Control-B (figure 1(c)), suggesting that BIAA may alter TCO_2 drawdown patterns. The differences in pH, CO_2, HCO_3^-, and CO_3^{2-} seen between Control-B and BIAA-B during the transition from lag phase (days 0–3) to exponential phase (days 3–9) suggest that biological activity strongly governed the carbonate chemistry in the BIAA treatments.

4.2. Alterations in biogeochemistry and physiological performance

In the biotic BIAA treatments, with a TA of 3000 μmol kg^{-1}, we observed short-term alterations, likely during the acclimation phase of growth, in five of the six measured biogeochemical and physiological parameters relative to control treatments. However, by day 6, only BSi remained consistently lower and PIC remained higher during the exponential phase of growth in the BIAA treatments. While POC, PON, F_v/F_m and FixArea were diminished only in BIAA-B relative to Control-B in the initial phases

of growth (acclimation/lag phase), differentially low BSi in BIAA-B was detected on day 3 and continue to the end of the experiment. Drops in F_v/F_m and FixArea (figure 2(f)) at the end of the experiment were coincidental with dissolved inorganic nutrients being extremely low or below detection limit by day 12 (figure 3).

Our results indicate that alkalinization via BIAA directly or indirectly altered the composition of a phytoplankton community and biogeochemically important parameters that represent two key functional processes in marine phytoplankton—silicification and calcification. As our experimental setup did not likely exclude all zooplankton grazers, the reduced diatom response (based on observed lower numbers of diatom cells and reduced BSi values in the BIAA treatment) could be explained by direct or indirect treatment impacts. For example, the reduced diatom numbers observed in the BIAA treatment might be a result of BIAA having a direct effect on phytoplankton physiological performance and ecological fitness or BIAA impacting zooplankton such as to cause an indirect impact on diatoms via altered grazing pressure. Our observed reduced BSi build up in the BIAA treatments is in agreement with results by Ferderer *et al* [11] using $NaHCO_3$ and NaOH (figure 2(a)).

Disruption to both magnitude and temporal trends of biogeochemical parameters, such as C:N ratios, was reported by Ferderer and colleagues (2022) who examined the impacts of $NaHCO_3$ and NaOH-based alkalinity addition upon natural phytoplankton communities [11]. While we did not observe an association between BIAA treatment and delayed increase of POC:PON during the exponential phase of growth, BIAA-B and Control-B displayed noticeably different POC:PON temporal patterns with highest average POC:PON value for BIAA-B occurring on day 9 (14.28 ± 1.98 μm) and for Control-B occurring on day 12 (17.48 ± 0.92 μm) (figure S1(c)). Our PIC and BSi results may suggest that BIAA under nutrient replete conditions could promote the growth of calcifiers and disadvantage silicifiers in a population dominated by diatoms, typical of a spring upwelling event (figure 4).

4.3. Trends in dissolved seawater nutrients

All treatments had measured pH values of 7.9–8.9 throughout the course of sampling (figure 1) which fall within the noted 7.2–9.1 pH window in which phosphate has been observed to precipitate out of seawater, often in association with Mg and Ca [57]. Nucleation rates of some phosphate-based precipitates are lessened in seawater conditions experiencing lower comparative pH values [57], and the likelihood of phosphate precipitation is supported by SEM-EDX data which showed that on days 6 and 12 aggregate particles from BIAA-A were composed primarily of P, Fe, O, Mg and Si (figure S2), in agreement with observations of phosphate precipitation based on SEM-EDX results from Gately *et al* [8].

Our observation of perturbed nutrient dynamics (for example, BSi:POC ratios) is supported by Ferderer et al's findings using a non Mg-containing alkali treatment which altered the Si:N ratios, as well as both the absolute BSi and N values and temporal trends of phosphate and silicate concentrations [11]. Similarly, Gately *et al* observed reductions in dissolved silicate with increasing concentrations of Ca-based alkalinity addition [8]. Further, the incomplete silicate removal in BIAA-B compared to Control-B is consistent with the delayed silicate drawdown trends in Ferderer *et al*'s OAE treatment versus control [11]. Correspondingly, the more complete drawdown of silicate in Control-B relative to BIAA-B is consistent with the higher comparative values of BSi in Control-B relative to BIAA-B (figure 2(a)).

Our results are in agreement with previous works that show that high alkalinity levels can induce secondary precipitation [53–55, 57], thus reducing alkalinity, thereby lowering mCDR potential and removing important nutrients from solution [8]. Hartmann *et al* observed such 'runaway precipitation' with brucite introduction under both oligotrophic abiotic and biotic conditions [58] while Yang *et al* found that 'runaway precipitation' is not an inevitable result of $Mg(OH)_2$-enhancement [59]. While we did not observe 'runaway precipitation' (figures 1(a)), our BIAA treatment was associated with increased particulate formation (figure S2) under abiotic conditions without concomitant significantly different dissolved silicate, phosphate, or nitrite + nitrate trends (figure 3 (c), (d), (g), (h), (k) and (l)). When considered alongside the altered dissolved nutrient dynamics (figures 3(a), (b), (e), (f), (i) and (j)) and BSi production (figure 2(a)) in biotic conditions with BIAA presence, our findings suggest that BIAA has likely impacted the physiological performance of some phytoplankton members.

Neither our study nor Ferderer *et al* [11] offer a mechanistic framework explaining how alkalinity additions changed the diatom community composition, reduced Si drawdown and BSi build up, and altered POC:PON ratios. Taxon-specificity in the responses of diatoms to alkalinization has been proposed in a recent study [60] although silicate might have been limited during part of the experiment. Our observations of altered dissolved silicate, phosphate, and nitrite + nitrate dynamics (figure 3) are in line with reduced BSi values and temporal changes to biogeochemistry and physiology observed in BIAA treatments (figure 2).

4.4. Phytoplankton community changes

Our results on phytoplankton community abundance contribute to discussions of competitive advantage of phytoplanktonic silicifiers and calcifiers, especially when considering possible future ocean regimes [61, 62]. While diatoms remained the dominant functional group throughout the experiment in both biotic treatments, their relative proportion within the phytoplankton community was lower while the relative proportion of coccolithophores and *Phaeocystis sp*. was higher in BIAA-B compared to Control-B (figures 4(b) and (c)), thus showing preferential selection of Prymnesiophytes over diatoms in BIAA-B.

As previous works have established that coccolithophore species can dominate under semioligotrophic conditions of low dissolved inorganic nutrients [39, 63, 64], the observation of increasing or plateaued coccolithophore counts (figure 4(a)) concurrent with decreasing dissolved nutrient concentrations (figure 3) is unsurprising although coccolithophores never reached bloom conditions [64] in either Control-B or BIAA-B, but were instead found at cell densities previously established as within expected ranges for southern California coastal waters [65, 66].

5. Conclusions

The phytoplankton community within our experiment was altered in response to BIAA, even at TA concentrations considered to be 'moderate' for OAE deployment scenarios. Additionally, BIAA was associated with overall reductions in BSi, and perturbed temporal trends in most of our measured biogeochemical and physiological parameters (BSi, POC, PON, F_v/F_m and FixArea).

Our results indicate that Prymnesiophyceae were preferentially selected under BIAA treatment while the response of dinoflagellates remains unclear. The lower contribution of diatoms to the phytoplankton community throughout the experiment is reflected by the reduced BSi values and the decreased dissolved silicate drawdown shown in BIAA-B compared to Control-B over time, which agrees in part with previous work using various sources of alkalinity [8, 11].

Though limited statistical power of laboratory studies necessitates nuanced application of our results to other systems, our study reinforces emerging knowledge regarding the reciprocal interactions between phytoplankton functions and alkalinity additions, and the interspecific variability that exists therein [8–11, 61]. Our results indicate that BIAA caused multi-faceted impacts ultimately resulting in alterations in community structure, biogeochemistry, physiology, and patterns of nutrient uptake and biomineralization that lasted at least until the cultures reached the stationary phase of growth. This work contributes to our understanding of the benefits and risks of OAE, and underscores the urgent need to consider biological impacts when proposing or planning field deployments.

Data availability statement

The data that support the findings of this study are openly available at the following URL/DOI: https://doi.org/10.5061/dryad.9cnp5hqvk [67].

Acknowledgment

The authors would like to thank the following individuals and organizations for their support and advice with regards to chemical analysis (C. Yorke, UCSB), materials and instrument access (A. Ritger, G. Hofmann Lab, UCSB) and experimental setup (J. Gately). This work was funded by the UCSB Coastal Fund (Grant ID *CF-202204-02452* to Welch; Grant ID *CF-202311-08493* to Welch and Liu), the Department of Energy to Iglesias-Rodriguez and Carbon To The Sea to Iglesias-Rodriguez.

ORCID iDs

Zoë S Welch 0009-0008-3023-3047
Sylvia M Kim 0000-0002-4534-5817
Michael Liu 0009-0007-8795-5254
An Bui 0000-0002-9548-7776
Janice L Jones 0000-0003-1655-297X
M Débora Iglesias-Rodríguez 0000-0001-9474-602X

References

[1] Keeling C D, Bacastow R B, Bainbridge A E, Ekdahl Jr C A, Guenther P R, Waterman L S and Chin J F S 1976 Atmospheric carbon dioxide variations at Mauna Loa observatory, Hawaii *Tellus* **28** 538–51
[2] Arrhenius S 1896 On the influence of carbonic acid in the air upon the temperature of the ground *Lond Edinb Dublin Philos Mag J Sci* **41** 237–76
[3] Pearson P N and Palmer M R 2000 Atmospheric carbon dioxide concentrations over the past 60 million years *Nature* **406** 695–9
[4] Zeebe R E, Ridgwell A and Zachos J C 2016 Anthropogenic carbon release rate unprecedented during the past 66 million years *Nat Geosci* **9** 325–9
[5] Manabe S and Wetherald R T 1967 Thermal equilibrium of the atmosphere with a given distribution of relative humidity *J Atmospheric Sci* **24** 241–59
[6] Held I M and Soden B J 2006 Robust responses of the hydrological cycle to global warming [cited 9 Jun 2024] (available at: https://journals.ametsoc.org/view/journals/clim/19/21/jcli3990.1.xml)
[7] Fakhraee M, Li Z, Planavsky N and Reinhard C 2023 A biogeochemical model of mineral-based ocean alkalinity enhancement: impacts on the biological pump and ocean carbon uptake *Environ. Res. Lett.* **18** 4
[8] Gately J A, Kim S M, Jin B, Brzezinski M A and Iglesias-Rodriguez M D 2023 Coccolithophores and diatoms resilient to ocean alkalinity enhancement: a glimpse of hope? *Sci. Adv.* **9** eadg6066
[9] Guo J A, Strzepek R F, Swadling K M, Townsend A T and Bach L T 2024 Influence of ocean alkalinity enhancement

with olivine or steel slag on a coastal plankton community in Tasmania *Biogeosciences* **21** 2335–54
[10] Ramírez L, Pozzo-Pirotta L J, Trebec A, Manzanares-Vázquez V, Díez J L and Arístegui J 2025 Ocean alkalinity enhancement (OAE) does not cause cellular stress in a phytoplankton community of the sub-tropical Atlantic Ocean *Biogeosciences* **22** 1865–86
[11] Ferderer A, Chase Z, Kennedy F, Schulz K G and Bach L T 2022 Assessing the influence of ocean alkalinity enhancement on a coastal phytoplankton community *Biogeosciences* **19** 5375–99
[12] Caserini S, Storni N and Grosso M 2022 The availability of limestone and other raw materials for ocean alkalinity enhancement *Glob. Biogeochem.* **36** e2021GB007246
[13] Merrill A M 2022 Magnesium Compounds 2018 *2018 Miner Year* (United States Geological Survey)
[14] Simandl G, Paradis S and Irvine M 2007 Brucite—industrial mineral with a future *Geosci. Can.* **34** 57–64
[15] Lenton A, Matear R J, Keller D P, Scott V and Vaughan N E 2017 Assessing carbon dioxide removal through global and regional ocean alkalization under high and low emission pathways (available at: https://esd.copernicus.org/preprints/esd-2017-92/esd-2017-92.pdf) (Accessed 9 October 2024)
[16] Bertagni M B and Porporato A 2022 The carbon-capture efficiency of natural water alkalinization: implications for enhanced weathering *Sci. Total Environ.* **838** 156524 (Accessed 12 June 2024)
[17] He J and Tyka M D 2023 Limits and CO_2 equilibration of near-coast alkalinity enhancement *Biogeosciences* **20** 27–43
[18] Delacroix S, Nystuen T J, Höglund E and King A L 2023 Biological impact of ocean alkalinity enhancement of magnesium hydroxide on marine microalgae using bioassays simulating ship-based dispersion (available at: https://bg.copernicus.org/preprints/bg-2023-138/) (Accessed 12 June 2024)
[19] Dickson A G 2010 The carbon dioxide system in seawater: equilibrium chemistry and measurements. Guide to best practices for ocean acidification research and data reporting vol 1 (Publications Office of the European Union) pp 17–40
[20] Brzezinski M A and Washburn L 2011 Phytoplankton primary productivity in the Santa Barbara Channel: effects of wind-driven upwelling and mesoscale eddies *J. Geophys. Res. Oceans* **116** C12
[21] Simons R D and Catlett D 2023 Regulation of a surface chlorophyll hotspot by wind-driven upwelling and eddy circulation in the Santa Barbara Channel, Southern California *Prog. Oceanogr.* **217** 103096
[22] Kroeker K J, Bell L E, Donham E M, Hoshijima U, Lummis S, Toy J A and Willis-Norton E 2020 Ecological change in dynamic environments: accounting for temporal environmental variability in studies of ocean change biology *Glob. Change Biol.* **26** 54–67
[23] Kessouri F, Renault L, McWilliams J C, Damien P and Bianchi D 2022 Enhancement of oceanic eddy activity by fine-scale orographic winds drives high productivity, low oxygen, and low pH conditions in the Santa Barbara Channel *J. Geophys. Res. Oceans* **127** e2022JC018947
[24] Sandoval-Belmar M, Smith J, Moreno A R, Anderson C, Kudela R M, Sutula M, Kessouri F, Caron D A, Chavez F P and Bianchi D 2023 A cross-regional examination of patterns and environmental drivers of Pseudo-nitzschia harmful algal blooms along the California coast *Harmful Algae* **126** 102435
[25] Kapsenberg L and Hofmann G E 2016 Ocean pH time-series and drivers of variability along the northern C hannel I slands, C alifornia, USA *Limnol. Oceanogr.* **61** 953–68
[26] Hendershott M C and Winant C D 1996 Surface circulation in the Santa Barbara channel *Oceanography* **9** 114–21
[27] Aristizábal M F, Fewings M R and Washburn L 2016 Contrasting spatial patterns in the diurnal and semidiurnal temperature variability in the Santa Barbara Channel, California *J. Geophys. Res. Oceans* **121** 427–40
[28] Hofmann G E *et al* 2011 High-frequency dynamics of ocean pH: a multi-ecosystem comparison *PLoS One* **6** e28983
[29] Renforth P and Henderson G 2017 Assessing ocean alkalinity for carbon sequestration *Rev. Geophys.* **55** 636–74
[30] Ilyina T, Wolf-Gladrow D, Munhoven G and Heinze C 2013 Assessing the potential of calcium-based artificial ocean alkalinization to mitigate rising atmospheric CO2 and ocean acidification *Geophys. Res. Lett.* **40** 5909–14
[31] Guillard R R L and Ryther J H 1962 Studies of marine planktonic diatoms. I. cyclotella nana hustedt, and detonula confervacea (cleve) gran *Can. J. Microbiol.* **8** 229–39
[32] Langer G, Geisen M, Baumann K-H, Kläs J, Riebesell U, Thoms S and Young J R 2006 Species-specific responses of calcifying algae to changing seawater carbonate chemistry *Geochem. Geophys. Geosyst.* **7** 9
[33] Iglesias-Rodríguez M D, Rickaby R E M, Singh A and Gately J A 2023 Laboratory experiments in ocean alkalinity enhancement research *State Planet* **2-oae2023** 1–18
[34] Dickson A G, Sabine C L and Christian J R 2007 Guide to best practices for ocean CO2 measurements (North Pacific Marine Science Organization) (available at: https://repository.oceanbestpractices.org/handle/11329/249) (Accessed 10 June 2024)
[35] Clayton T D and Byrne R H 1993 Spectrophotometric seawater pH measurements: total hydrogen ion concentration scale calibration of *m*-cresol purple and at-sea results *Deep-Sea Res.* **40** 2115–29
[36] Lewis E R and Wallace D W R 1998 Program developed for CO2 system calculations. environmental system science data infrastructure for a virtual ecosystem (ESS-DIVE) (United States) *Report No.: cdiac:CDIAC-105* (available at: www.osti.gov/dataexplorer/biblio/dataset/1464255) (Accessed 10 June 2024)
[37] Mehrbach C, Culberson C H, Hawley J E and Pytkowicx R M 1973 Measurement of the apparent dissociation constants of carbonic acid in seawater at atmospheric pressure1 *Limnol. Oceanogr.* **18** 897–907
[38] Dickson A G and Millero F J 1987 A comparison of the equilibrium constants for the dissociation of carbonic acid in seawater media *Deep-Sea Res.* **34** 1733–43
[39] Matson P G, Washburn L, Fields E A, Gotschalk C, Ladd T M, Siegel D A, Welch Z S and Iglesias-Rodriguez M D 2019 Formation, development, and propagation of a rare coastal coccolithophore bloom *J. Geophys. Res. Oceans* **124** 3298–316
[40] Paasche E 1973 Silicon and the ecology of marine plankton diatoms. I. Thalassiosira pseudonana (Cyclotella nana) grown in a chemostat with silicate as limiting nutrient *Mar Biol* **19** 117–26
[41] Brzezinski M A and Nelson D M 1995 The annual silica cycle in the Sargasso Sea near Bermuda *Deep-Sea Res.* **42** 1215–37
[42] Krause J W, Nelson D M and Lomas M W 2009 Biogeochemical responses to late-winter storms in the Sargasso Sea, II: increased rates of biogenic silica production and export *Deep-Sea Res.* **56** 861–74
[43] Thwe A A and Kasemsap P 2014 Quantification of OJIP fluorescence transient in tomato plants under acute ozone stress *Agric. Nat. Resour.* **48** 665–75
[44] Yunus M, Pathre U and Mohanty P 2014 *Probing Photosynthesis: Mechanism, Regulation & Adaptation* (CRC Press) p 579
[45] Graupner N, Röhl O, Jensen M, Beisser D, Begerow D and Boenigk J 2017 Effects of short-term flooding on aquatic and terrestrial microeukaryotic communities: a mesocosm approach *Aquat. Microb. Ecol.* **80** 257–72
[46] Schagerl M, Siedler R, Konopáčová E and Ali S S 2022 Estimating biomass and vitality of microalgae for monitoring cultures: a roadmap for reliable measurements *Cells* **11** 2455

[47] Sieber G, Beisser D, Rothenberger J L, Shah M, Schumann M, Sures B and Boenigk J 2022 Microbial community shifts induced by plastic and zinc as substitutes of tire abrasion *Sci. Rep.* **12** 18684
[48] Meissel K and Yao E S 2024 Using cliff's delta as a non-parametric effect size measure: an accessible web app and R tutorial *Pract. Assess. Res. Eval.* **29** 2
[49] Wobbrock J O, Findlater L, Gergle D and Higgins J J 2011 The aligned rank transform for nonparametric factorial analyses using only anova procedures *Proc. SIGCHI Conf. on Human Factors in Computing Systems* (ACM) pp 143–6
[50] Kay M, Elkin L A, Higgins J J and Wobbrock J O 2021 ARTool: aligned rank transform (available at: https://cran.r-project.org/web/packages/ARTool/index.html) (Accessed 3 November 2024)
[51] Cohen J 1988 *Statistical Power Analysis for the Behavioral Sciences* 2nd edn(Routledge) p 567
[52] Parkhill J-P, Maillet G and Cullen J J 2001 Fluorescence-Based maximal quantum yield for PSII as a diagnostic of nutrient stress *J. Phycol.* **37** 517–29
[53] Salimi M H, Heughebaert J C and Nancollas G H 1985 Crystal growth of calcium phosphates in the presence of magnesium ions *Langmuir* **1** 119–22
[54] Cappellen P V and Berner R A 1991 Fluorapatite crystal growth from modified seawater solutions *Geochim. Cosmochim. Acta* **55** 1219–34
[55] Abbona F and Franchini-Angela M 1990 Crystallization of calcium and magnesium phosphates from solutions of low concentration *J. Cryst. Growth* **104** 661–71
[56] Oschlies A, Stevenson A, Bach L T, Fennel K, Rickaby R E M, Satterfi Eld T, Webb R and Gattuso J-P (eds) 2023 *Guide to Best Practices in Ocean Alkalinity Enhancement Research (OAE Guide 23)* vol **2** (Copernicus Publications, State Planet)
[57] Golubev S V, Pokrovsky O S and Savenko V S 1999 Unseeded precipitation of calcium and magnesium phosphates from modified seawater solutions *J. Cryst. Growth* **205** 354–60
[58] Hartmann J *et al* 2023 Stability of alkalinity in ocean alkalinity enhancement (OAE) approaches—consequences for durability of CO_2 storage *Biogeosci. Discuss.* **2022** 1–29
[59] Yang B, Leonard J and Langdon C 2023 Seawater alkalinity enhancement with magnesium hydroxide and its implication for carbon dioxide removal *Mar. Chem.* **253** 104251
[60] Ferderer A, Schulz K G, Riebesell U, Baker K G, Chase Z and Bach L T 2024 Investigating the effect of silicate- and calcium-based ocean alkalinity enhancement on diatom silicification *Biogeosciences* **21** 2777–94
[61] Wang J, Zeng C and Feng Y 2024 Meta-analysis reveals responses of coccolithophores and diatoms to warming *Mar.Environ. Res.* **193** 106275
[62] Hutchins D A, Fu F-X, Yang S-C, John S G, Romaniello S J, Andrews M G and Walworth N G 2023 Responses of globally important phytoplankton species to olivine dissolution products and implications for carbon dioxide removal via ocean alkalinity enhancement *Biogeosciences* **20** 4669–82
[63] Iglesias-Rodriguez M D, Armstrong R, Feely R, Hood R, Kleypas J, Milliman J D, Sabine C and Sarmiento J 2002 Progress made in study of ocean's calcium carbonate budget *EOS Trans. Am. Geophys. Union* **83** 365–75
[64] Tyrrell T and Merico A 2004 Emiliania huxleyi: bloom observations and the conditions that induce them ed H R Thierstein and J R Young *Coccolithophores* (Springer) pp 75–97 (available at: http://link.springer.com/10.1007/978-3-662-06278-4_4)
[65] Winter A 1985 Distribution of living coccolithophores in the California Current system, southern California borderland *Mar. Micropaleontol.* **9** 385–93
[66] Ziveri P, Thunell R C and Rio D 1995 Seasonal changes in coccolithophore densities in the Southern California Bight during 1991–1992 *Deep-Sea Res.* **42** 1881–903
[67] Welch Z *et al* 2025 *Data from: Brucite-Inspired Ocean Alkalinity Enhancement Alters the Biogeochemistry and Composition of a Phytoplankton Community: A Santa Barbara Channel Case Report [Dataset]* (Dryad) (https://doi.org/10.5061/dryad.9cnp5hqvk)